RESEARCH

Activation of anthracite combustion by copper acetate: mechanism, effect of particle size and introduction method

K. B. Larionov[1,2] · I. V. Mishakov[3] · N. I. Berezikov[1,2] · A. S. Gorshkov[1,2] · A. Zh. Kaltaev[1] · K. V. Slyusarskiy[1,2] · A. S. Ruban[1] · A. A. Vedyagin[3]

Abstract

This paper addressed the effect of copper acetate on the combustion characteristics of anthracite depending on the fractional composition of fuel and additive introduction method. Anthracite was impregnated with 5 wt% of $Cu(CH_3COO)_2$ by mechanical mixing and incipient wetness impregnation. Four anthracite samples of different fraction with $d < 0.1$ mm, $d = 0.1–0.5$ mm, $d = 0.5–1.0$ mm, and $d = 1.0–2.0$ mm were compared. According to EDX mapping, incipient wetness impregnation provides a higher dispersion of the additive and its uniform distribution in the sample. The ignition and combustion characteristics of the modified anthracite samples were studied by thermal analysis and high-speed video recording of the processes in a combustion chamber (at heating medium temperature of 800 °C). It was found that copper acetate increases anthracite reactivity, which was evidenced by decreased onset temperature of combustion (ΔT_i) by 35–190 °C and reduced ignition delay time ($\Delta \tau_i$) by 2.1–5.4 s. Copper acetate reduces fuel underburning (on average by 70%) in the ash residue of anthracite and decreases the amount of CO and NO_x in gas-phase products (on average by 18.5% and 20.8%, respectively). The mechanism for activation of anthracite combustion by copper acetate is proposed.

Keywords Anthracite · Copper acetate · Fractional composition · Activation · Ignition · Combustion · Micro-explosions · Fuel underburning · Gas-phase products · Activation mechanism

1 Introduction

Renewable energy sources continue to be one of the rapidly developing research areas (British Petroleum 2020; IEA 2020, 2021) with the focus on the adopted carbon-free energy strategy (IEA 2021) initiated in different countries. However, coal, as an energy resource, remains one of the cheapest and most common fuels in the world. According to British Petroleum (2020), the share of coal consumption in 2020 for electricity generation amounted to 35.1%, which

was by 11.7% and 23.4% higher than that of natural gas and other energy sources, respectively.

However, widespread application of coal is limited by a number of factors, which include inertia of combustion, incompleteness of combustion, and formation of toxic gases (CO, NO_x, SO_2). Therefore, the urgent challenge the coal energy currently faces is to improve methods of energy-based coal conversion or develop the new ones. There are different promising technological solutions developed for improving ecological and performance characteristics of coal-fired equipment. It could be relatively simple solutions like flue gas recirculation (de las Obras-Loscertales et al. 2013), swirl, staged (Zhang et al. 2022) and MILD (moderate, intense or low dilution) (Hu et al. 2019) combustion, as well as very complex projects requiring significant rearrangement or even substitution of major equipment like gasification or chemical looping combustion (Ryabov 2022). All of them require at least some modernization and adjustment of the boiler itself. Catalytic combustion of coal is one of the methods aimed at improving both environmental and energy performance (Ismagilov and Kerzhentsev 1999;

✉ K. B. Larionov
   laryk070@gmail.com

1 Energy Engineering School, National Research Tomsk
   Polytechnic University, Lenin Ave., 30, Tomsk 634050,
   Russia

2 Gorbachev Kuzbass State Technical University,
   Kemerovo 650000, Russia

3 Boreskov Institute of Catalysis SB RAS,
   Novosibirsk 630090, Russia

Simonov et al. 2013; Parmon et al. 2015), which could be implemented without changes in the boiler construction.

This method employs activating additives based on metal oxides (Gong et al. 2010a, 2010b; Zhao et al. 2011; Pinchuk and Kuzmin 2020; Zhang et al. 2020; Lei et al. 2021b, 2021a), as well as their precursors in the form of salts (He et al. 2013; Abbasi-Atibeh and Yozgatligil 2014). These agents increase the degree of fuel conversion at a relatively low temperature (Ismagilov and Kerzhentsev 1999; Parmon et al. 2015), decrease the nitrogen oxide concentration in the exhaust gases (Ismagilov and Kerzhentsev 1999; Parmon et al. 2015), and provide more complete oxidation of carbon monoxide (AlKetbi et al. 2020; Riley et al. 2020). The major distinguishing feature of catalytic combustion in comparison with the conventional one is that oxidation of organic matter and CO proceeds mainly on the surface of the heterogeneous catalyst without flame formation (Li et al. 2009; Parmon et al. 2015).

Gong et al. (2010a) found that coals with the highest carbon content show the greatest catalytic effect evidenced by reduced temperature of intensive oxidation onset. This effect is due to a high content of oxygen-containing functional groups, the number of which decreases as the degree of metamorphism of solid fuels grows. Thus, catalytic combustion is mainly observed for fuels with a high carbon content and low reactivity (Gong et al. 2010a, 2010b; Gong and Zhang 2017; Yang et al. 2019), for example, anthracite. The development of the catalytic combustion technology will improve the efficiency of power equipment during start-up and operation (Simonov et al. 2013; Zou et al. 2016), and its ecological performance (Köpsel and Halang 1997; Yang et al. 2019).

Metal oxides should be considered as the most technologically appropriate option due to their effect during combustion. One of the examples is adding active metal oxides to a thermally stable carrier (for example, Al_2O_3 (Parmon et al. 2015)) which is subsequently used as fixed honeycomb blocks in a pseudo-liquefaction layer (Fedorov et al. 2021). However, for these systems, it is fundamentally important to ensure the dynamic contact of the catalytic system with fuel, which cannot be provided in fixed bed combustion.

An alternative option for catalytic combustion includes the development of combustion modifiers using transition metal salts as oxide precursors. A number of authors (ZHANG et al. 2014; Guo et al. 2014; Pinchuk and Kuzmin 2020) reported that salts added allow adjustment of oxidation parameters in a wide range. These parameters include the degree of conversion, the initial and final combustion temperature, the activation energy and the total thermal conversion time. Activation of the oxidation reaction is associated with the staged decomposition of salts and subsequent formation of metal oxides. The latter (for example, copper

oxide (Zhang et al. 2020)) were found to be an effective combustion catalyst for different energy systems.

In Larionov et al. (2020), it was reported that nitrate and copper acetate used as an activating additive has a positive effect on the anthracite combustion characteristics. The increased fuel reactivity was evidenced by reduced ignition delay time and decreased ignition temperature. The greatest activity was recorded for copper acetate used as an initiating agent.

Currently, most of the studies addressing oxidation and combustion activated using oxides and their precursors employ the thermogravimetric analysis method. In this case, fuel powders are used as study objects with the particle size of less than 100 μm. These conditions differ significantly from the real fixed bed combustion of coal in power equipment, and this hampers practical application of the obtained results. Thus, the aim of the present study was to determine the activation mechanism and to study the effect of the fractional composition of fuel and additive introduction methods (metal oxide precursor) on combustion characteristics in the activation mode. The experimental methodology used allows investigation of the process directly in a combustion chamber using visualizing devices (high-speed video recording) to determine the most appropriate method of additive introduction and predict the behavior of the modified fuel during its combustion in fuel-burning equipment. The experiments employed scanning electron spectroscopy, thermal analysis, and high-speed video recording.

This study presents experimental results on the effect of $Cu(CH_3COO)_2$ activating additive applied by different methods on the reactivity of different fractions of anthracite in conditions of thermal analysis and experimental combustion setup. The major ignition and combustion characteristics were evaluated as well as major stages of process and composition of gas-phase products. The mechanism of additive action and possible ways of copper recovery were proposed.

2 Materials and methods

2.1 Preparation and characteristics of anthracite

The initial sample was anthracite from the Krasnogorsk deposit (Kemerovo region, Russia). The sample (fraction size $d = 10$–50 mm) was ground in a ball mill; the grinding mode was as follows: the ball-to-powder ratio was 1:1, the grinding time was 4 h. After that, the ground sample was divided into four fractions with the following particle size: $d < 0.1$ mm, $d = 0.1$–0.5 mm, $d = 0.5$–1.0 mm and $d = 1.0$–2.0 mm.

Proximate analysis (humidity W, ash content A, volatile matter content V, lower heating value LHV and bulk density ρ_b) was performed according to ISO standards: ISO

589:2008 Hard coal. Determination of total moisture; ISO 1171:2010 Solid mineral fuels. Determination of ash; ISO 562:2010 Hard coal and coke. Determination of volatile matter; ISO 1928:2009 Solid mineral fuel. Determination of gross heating value and calculation of low heating value; ISO 23499:2008 Coal. Determination of bulk density.

Particle density (ρ_p) was determined by the pycnometry method using isopropyl alcohol. For determination of bulk density and particle density, the samples were dried at 105 °C for 24 h. The porosity of the particle layer was calculated using the following formula:

$$\varepsilon_o = 1 - \rho_b/\rho_p \qquad (1)$$

The results are presented in Table 1.

The anthracite sample is characterized by a high ash content and relatively low content of volatile matter (Table 1), which is typical of fuels with a high degree of metamorphism (Wang et al. 2011). The higher content of ash in the sample with a particle size less than 0.1 mm can be associated with the components present in the inorganic part of the initial sample, which exhibit a higher abrasion rate compared to the organic part of anthracite.

Figure 1 presents the images of anthracite particles obtained by JSM-6000C scanning electron microscope (JEOL, Japan).

As can be seen in Fig. 1, anthracite particles are of irregular shape, and their surface is inhomogeneous. It should be noted that the size of particles in each sample was in the range specified by the fractional composition. A number of smaller fragments (less than 5 μm in size) can be observed on the surface of particles less than 0.1 mm in size (Fig. 1a). The value of the bulk density and, consequently, the value of porosity differ significantly

Table 1 Technical characteristics and elemental composition of anthracite

Characteristics	Fraction size (mm)			
	$d < 0.1$	$d = 0.1–0.5$	$d = 0.5–1.0$	$d = 1.0–2.0$
Humidity W^a (wt%)	1.4 ± 0.1	1.4 ± 0.2	1.0 ± 0.1	1.1 ± 0.1
Ash content A^d (wt%)	16.9 ± 0.5	10.1 ± 0.2	9.4 ± 0.2	9.8 ± 0.3
Volatile matter content V^{daf} (wt%)	6.8 ± 0.2	6.4 ± 0.3	5.8 ± 0.3	6.1 ± 0.2
Lower heating value (LHV) (MJ/kg)	25.9 ± 0.1	27.4 ± 0.1	28.0 ± 0.2	27.9 ± 0.1
Bulk density ρ_b (g/cm³)	0.63 ± 0.02	0.77 ± 0.03	0.79 ± 0.02	0.80 ± 0.03
Particle density ρ_p (g/cm³)	1.55 ± 0.03			
Porosity of the layer (ε_o)	0.59	0.50	0.49	0.48

[a] Analytical mass basis, [d] Dry mass basis, [daf] Combustible ash free mass basis

Fig. 1 SEM images of anthracite particles of different fractions. **a** $d < 0.1$ mm **b** $d = 0.1–0.5$ mm **c** $d = 0.5–1.0$ mm **d** $d = 1.0–2.0$ mm
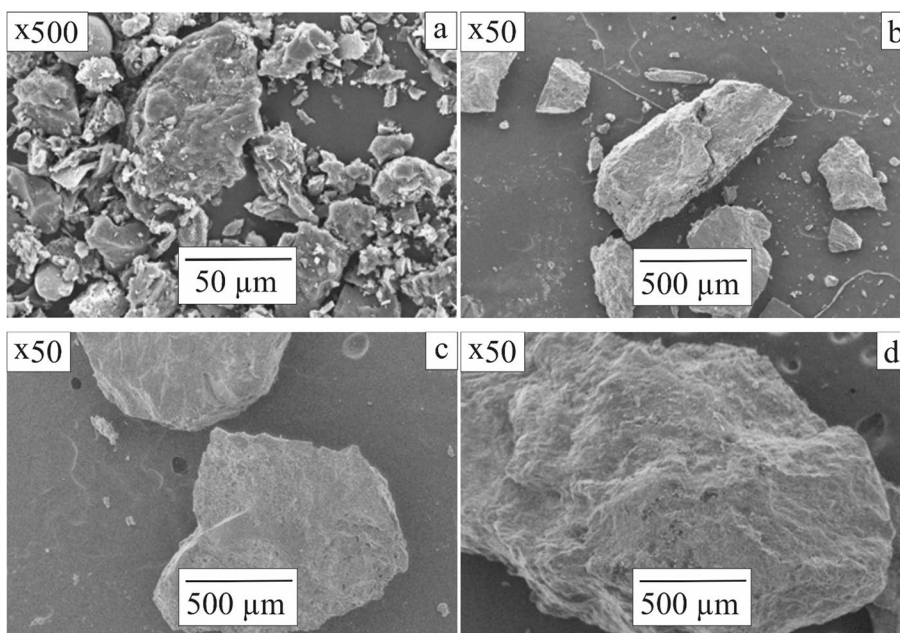
(Table 1), which is due to a large number of dispersed particles increasing the area of the friction surface.

2.2 Introduction of activating additives

Crystalline copper hydrate $Cu(CH_3COO)_2 \cdot H_2O$ (Richardson 2000) was used as an activating additive in the amount of 5 wt% (in terms of dry salt).

The additive was introduced in the anthracite sample using two methods: mechanical mixing and incipient wetness impregnation. The first method was realized by mixing the anthracite fractions with copper acetate in a laboratory pounder for 5 min. For incipient wetness impregnation, water-alcohol solution with a volumetric ratio $C_2H_5OH/H_2O = 50/50$ was used, a more detailed description of the method is given in (Tokareva et al. 2014). Ethanol in the impregnation solution helped overcome the problem of anthracite hydrophobicity. After that, all the samples modified with copper acetate were dried at 105 °C for 24 h.

Table 2 compares the elemental composition for the initial and modified anthracite samples (incipient wetness impregnation), which was determined using the Euro EA 3000 analyzer (EuroVector, Italy). The elemental composition was determined for the samples with the particle size less than 0.1 mm.

For the samples containing 5 wt% copper acetate-based additive, the ash content increases by 1.2 wt%, which is caused by cooper oxide formation. Addition of copper acetate also increases O/C and H/C ratios by 53.9% and 26.5%, respectively, which is caused by the nature of the additive used.

The additive distribution in the anthracite-based sample was studied by EDX mapping using the TESCAN VEGA3 scanning electron microscope (TESCAN ANALYTICS, France) and the X-Max 50 EDS adapter (Oxford Instruments, USA) with accelerating voltage of 10–20 kV, a sample current of 12 nA and a spot with $d = 2$ μm.

2.3 TG and MS analysis

Oxidation of the anthracite samples (and the ash residue formed after combustion) was investigated using the thermal analyzer STA 449 C Jupiter (Netzsch, Germany). All experiments were conducted at the air flow rate of 150 mL/min and the heating rate of 10 °C/min in an alumina crucible with a perforated lid in the temperature range of 25–1000 °C. The sample mass was about 10 mg. A qualitative compositional analysis of the gas-phase oxidation products was conducted. The analysis was carried out using the QMS 403 D Aëolos interfacing quadruple mass spectrometer (Netzsch, Germany). The ash residue was subjected to oxidation in order to determine the amount of fuel underburning.

The oxidation characteristics (initial and final temperature of the intensive oxidation T_i and T_f respectively, the maximum speed of the oxidation process w_{max} at temperature T_{max}) were determined by the graphic method using the TG and DTG data obtained (Zou et al. 2016). The kinetic analysis was performed using Coats-Redfern equation (Zhang et al. 2020):

$$\ln\left(\frac{G(\alpha)}{T_i^2}\right) = \ln\left(\frac{A \cdot R}{\beta \cdot E}\right) - \frac{E}{R \cdot T_i}$$

where, $G(\alpha)$ is integral conversion function; T_i is the temperature of reaching given α, K; A is the frequency factor, 1/s; R is the gas constant, J/(mol K); β is heating rate, K/s; E is the activation energy, J/mol.

2.4 Ignition and combustion

Figure 2 presents a schematic diagram of the experimental setup used to study ignition and combustion processes. It comprises the following components: a combustion chamber, namely a thermoregulated muffle furnace (Sputnik, Russia) with a power of 2 kW and a digital temperature controller (the rmocouple measurement error ± 3–5 °C) with a volume of 0.003 m^3; a high-speed video camera FAST-CAM SA4 5 (Photron, USA) with a 1024×1024 resolution at frame rate of 250 fps (parameters are relevant for the experiment); a remotely controlled coordinate mechanism; the flow gas analyzer Test-203 (BONER, Russia).

The experiment was conducted in two stages. In the temperature-controlled furnace, the heating medium temperature was $T_g = 800$ °C. The temperature in the furnace was measured using chromel–alumel thermocouple. A fuel sample with a weight of apporx. 0.10 ± 0.01 g was placed in a cylindrical form installed on a metal substrate. The metal substrate was attached to the tube with an internal diameter of 6 mm, which was, in turn, installed on the coordinate mechanism. Then, the form was removed

Table 2 Elemental composition of the initial anthracite sample and the sample modified by $Cu(CH_3COO)_2$ via incipient wetness impregnation

Sample	Elemental Composition* (wt%)							Ash content (wt%)
	C	H	N	S	O	O/C	H/C	
No additive	72.42 ± 0.3	1.58 ± 0.06	1.19 ± 0.08	0.21 ± 0.01	7.70	0.08	0.26	16.9 ± 0.5
5 wt% Cu $(CH_3COO)_2$	67.78 ± 0.1	1.87 ± 0.02	1.03 ± 0.04	0.13 ± 0.03	11.12	0.12	0.34	18.1 ± 0.6

* with respect to the dry mass

Fig. 2 Experimental setup for studying ignition and combustion of solid fuel
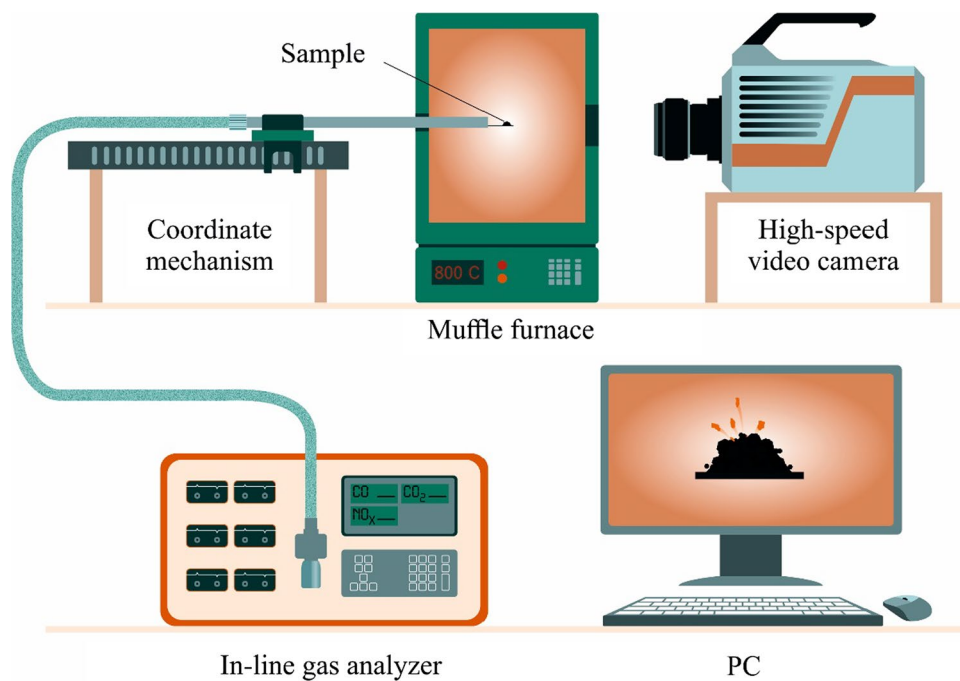
by a translational upward movement, as a result of which a cone-shaped filling was formed. Later, the coordinate mechanism with the fuel hitch was driven using a PC and moved to the center of the combustion chamber. At the time of launch of the coordinate mechanism, a high-speed video recording had begun, registering the ignition and subsequent combustion of the fuel hitch.

The gas-phase products formed during combustion (CO, CO_2, NO_x) passed through the tube and were analyzed by the flow gas analyzer. The flow rate of gases passing through the gas analyzer was 0.3 L/min. The sensor scanning time was 3 s. Relative measurement error was 5%.

A comparative assessment of the fuel reactivity was carried out using the values of the ignition delay time, which was obtained using high-speed video recording. The ignition delay time was the interval from the moment when the fuel holder entered the focus of the video camera to a visible glow on the fuel surface, which corresponds to the combustion onset. Using the Photon FastCam Viewer 4.0.3.2 Software (Photron, United States) allows seeing frame-by-frame the video sequence and fixing the input and the ignition of the sample. The difference in the frame numbers divided by the speed of video recording (the number of frames per second, which was 250) corresponded to the time of the ignition of the fuel.

The completion of the process was recorded by the flow gas analyzer, when the formation of gas-phase compounds (CO, CO_2, NO_x) stopped. Then, the ash residue was removed from the metal substrate and cooled in a ceramic container with no air access. At the end of the experiment, the gas analyzer and the furnace were blown with air to ensure measurement accuracy. At least ten experiments were carried out under the same conditions for each sample.

2.5 Statistical analysis

Test of Normality was performed by Kolmogorov–Smirnov test using STATISTICA 8.0 (StatSoftInc). The results of determination of oxidation parameters (T_i, T_f, w_{max}, T_{max}) and ignition delay time were evaluated by the Student's t-tests. Data were presented as M ± SD. The values were considered to be statistically significant with $p < 0.001$.

3 Results and discussion

3.1 Additive distribution

Figure 3 shows the EDX-mapped micrographs of anthracite particles (for sample fractions with $d = 0.5–1.0$ mm), which display the additive distribution in the composition and on the surface of the sample particles, depending on the method of its introduction.

Figure 3b shows that distribution of the mechanically introduced activating additive is non-uniform: the sample contains both large and small particles of copper acetate. In turn, incipient wetness impregnation (Fig. 3c) allows uniform additive distribution in the fuel. This is due to the additive dispersion, which depends on the type of the method used. Pre-dissolution of copper acetate in
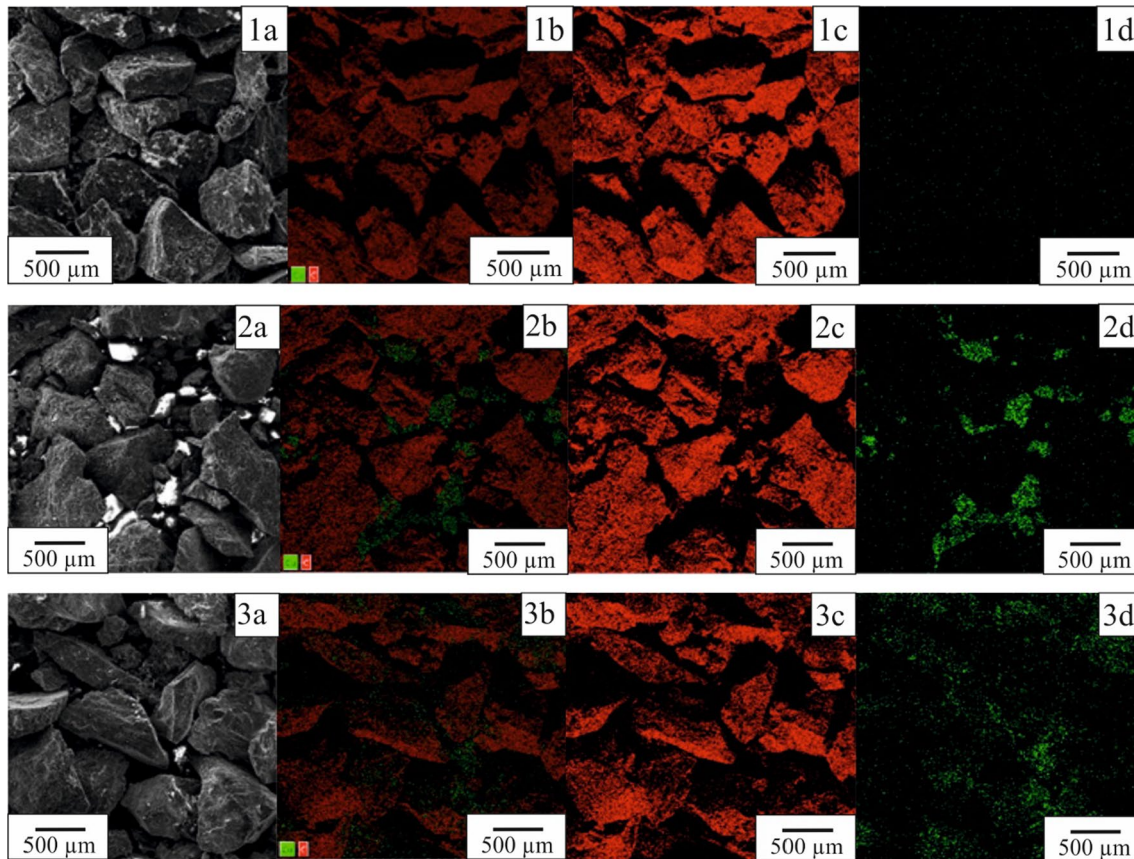
Fig. 3 SEM/EDX images of the anthracite samples with a fraction with $d = 0.5 – 1.0$ mm, 1 referes to reference sample, 2 refers to mechanical mixing, 3 refers to incipient wetness impregnation. **a** SEM **b** C/Cu **c** C (red) **d** Cu (green). Magnitude×100

water-alcohol solution increases the additive dispersion, which during fuel impregnation penetrates deeper into the particle structure consisting of pores and channels.

3.2 TG and MS analysis

Figure 4 shows the results obtained by the thermal analysis of the samples plotted in the form of TG and DTG curves. Table 3 presents the oxidation parameters of the sample calculated using the thermal analysis data.

The TG and DTG data suggest that intensive oxidation of the initial samples proceeds in two parallel stages associated with the release of volatile matter and oxidation of the carbon residue formed. The monomodal nature of the DTG profile during thermal decomposition of different fractional compositions of anthracite was also reported by Wu et al. (2019). It should be noted that the DSC curve (thermal effects) and the MS profile characterizing the CO_2 emission almost mirror the corresponding DTG profile for all samples (Fig. 4).

Regardless of the particle size, the TG and DTG profiles for the initial samples show a similar pattern in the

temperature range of 560–760 °C. This fact is obviously associated with the similarity of the chemical composition of the reactive part of different fractions and insignificant external and internal diffusion resistance of the fuel layer and particles. It should be noted that the amount of the ash residue formed correlates well with the data on technical characteristics of the samples (Table 1).

Using copper acetate as an activating additive has a significant effect on anthracite oxidation, which causes temperature drop at the onset and at the end of intense oxidation (T_i and T_f, respectively, Table 3).

The analysis has shown (Fig. 4) that additives intensify anthracite oxidation in the temperature range of 300–420 °C, which is due to copper acetate decomposition (Arii and Masuda 1999; Richardson 2000) on the anthracite particle surface. This significantly shifts the initial temperature of intensive oxidation to the low-temperature zone. As expected, the largest change in T_i is observed for the samples modified by incipient wetness impregnation. The maximum change in T_i and T_f was recorded for the sample with a minimum particle size (less than 0.1 mm) – 190 and 160 °C, respectively (Fig. 5). For an increased anthracite particles size, the
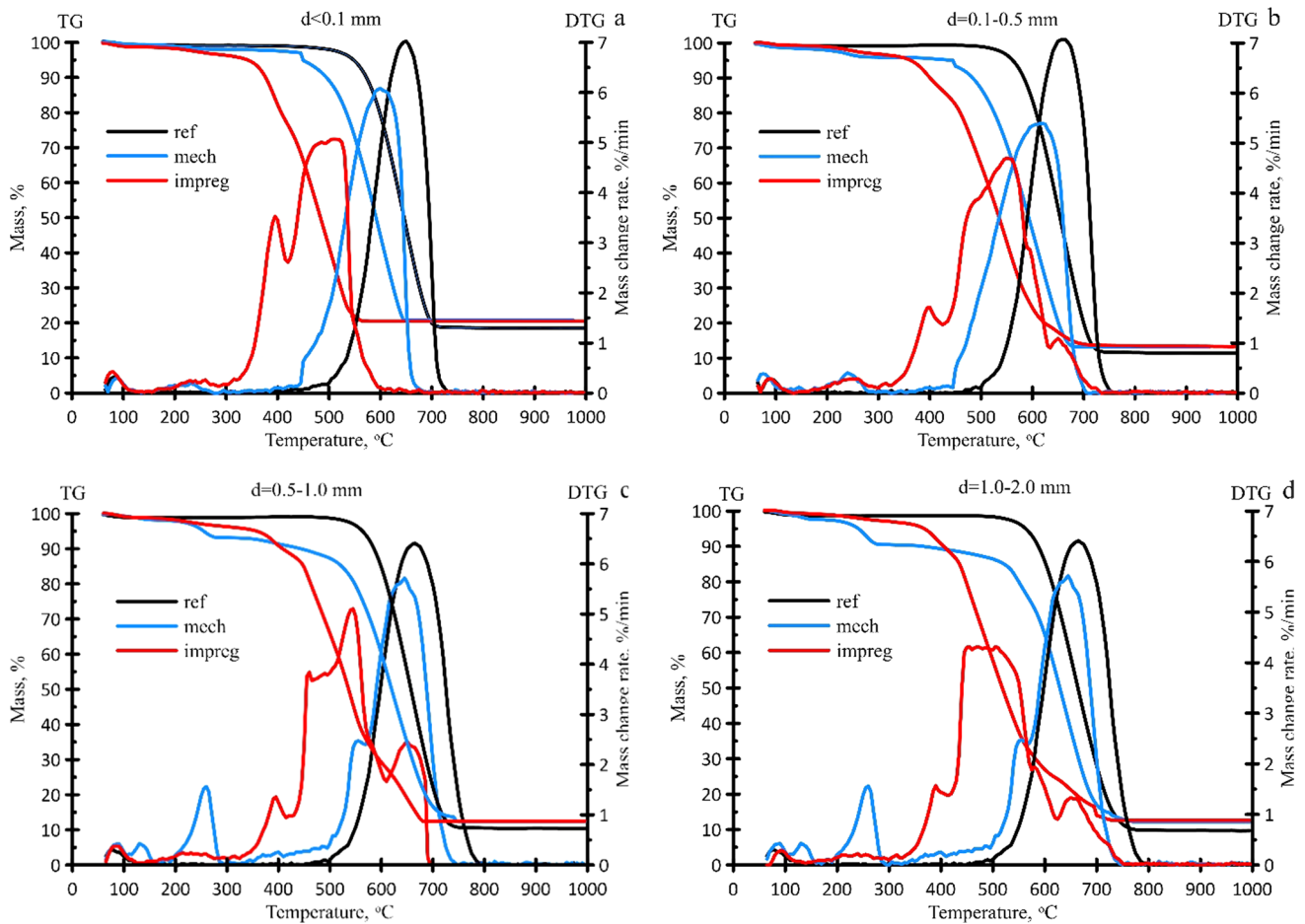
Fig. 4 TG and DTG data on oxidation of anthracite samples of different fraction **a** $d < 0.1$ mm **b** $d = 0.1$–0.5 mm **c** $d = 0.5$–1.0 mm **d** $d = 1.0$–2.0 mm. Note: ref means reference sample, mech means sample modified by mechanical activation method, impreg means sample modified by incipient wetness impregnation method. Air flow rate is 150 mL/min, heating rate is 10 °C/min, the sample weight is approx. 10 mg

Table 3 Oxidation parameters of the initial anthracite sample and modified samples of different fractions

Sample		T_i (°C)	T_f (°C)	w_{max} (%/min)	T_{max} (°C)	E (kJ/mol)
$d < 0.1$ mm	Ref	580 ± 3	700 ± 2	7.0 ± 0.1	645 ± 3	158
	Mech	500 ± 7	650 ± 4	6.1 ± 0.2	600 ± 7	118
	Impreg	390 ± 4	540 ± 5	5.1 ± 0.2	505 ± 11	64
$d = 0.1$–0.5 mm	Ref	580 ± 4	700 ± 6	7.1 ± 0.2	655 ± 8	157
	Mech	520 ± 9	660 ± 5	5.4 ± 0.3	620 ± 5	100
	Impreg	420 ± 5	610 ± 8	4.7 ± 0.2	545 ± 9	58
$d = 0.5$–1.0 mm	Ref	590 ± 3	715 ± 7	7.0 ± 0.1	660 ± 5	156
	Mech	540 ± 5	700 ± 4	5.2 ± 0.3	630 ± 5	105
	Impreg	460 ± 8	620 ± 3	5.1 ± 0.1	540 ± 3	54
$d = 1.0$–2.0 mm	Ref	595 ± 3	720 ± 6	6.4 ± 0.2	660 ± 4	142
	Mech	560 ± 7	700 ± 3	5.7 ± 0.3	640 ± 7	124
	Impreg	480 ± 8	630 ± 5	4.3 ± 0.1	500 ± 24	56

Statistically significant differences ($p < 0.001$) were established for all the fractions. The comparison was done for oxidation parameters between the following groups: ref/mech, ref/impreg, and mech/impreg
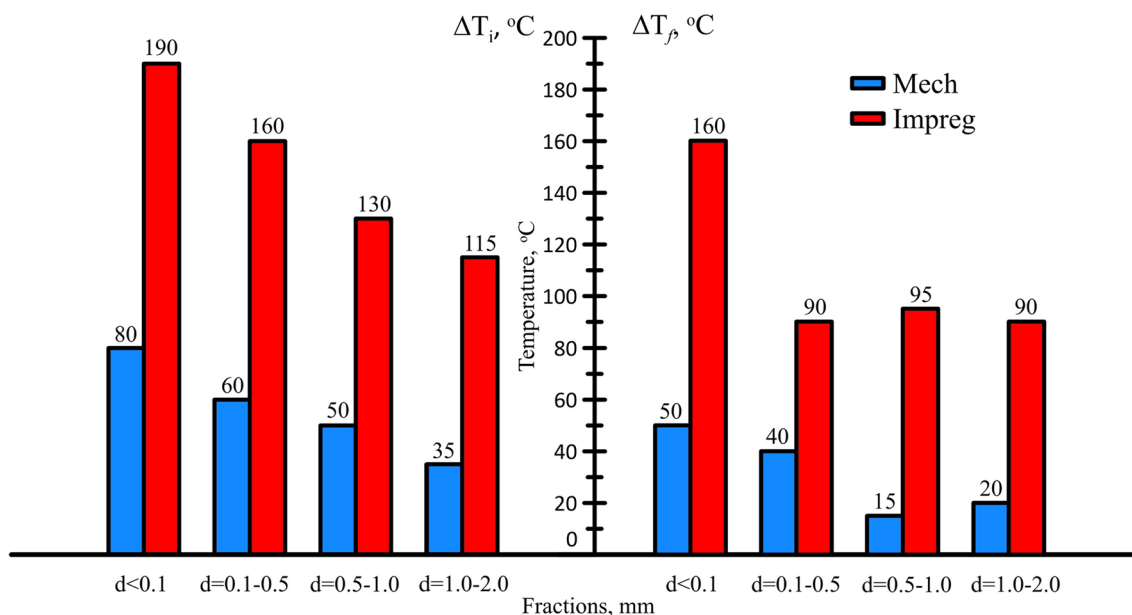
Fig. 5 Effect of the fractional composition and the method used for adding copper acetate on the temperature change at the onset of combustion (ΔT_i) and at the end of combustion (ΔT_f) of modified samples (TG data). mech – sample modified by mechanical activation method, impreg – sample modified by incipient wetness impregnation method

catalytic effect of the additive is observed to reduce through to decrease in the ΔT_i values (Fig. 5).

At the same time, it is worth noting that the use of copper acetate additive, unlike metals oxides (like iron oxide Gong et al. 2010a; Zhang et al. 2020)), contributes to a greater shift of the intensive oxidation process to the area of lower temperatures.

The DTG data show that oxidation of the modified samples has a number of specific characteristics expressed in the occurrence of two or more peaks on the DTG curves. A typical shift of DTG profiles to the low-temperature zone proportional to the change in T_i and T_f parameters should be noted. Additional peaks on the DTG profiles are attributed to the exothermic decomposition of copper acetate (according to the DSC data) in the low-temperature zone, subsequent release of the intensive volatile matter, and oxidation of the carbon residue formed. Zhang et al. (2005) studied the kinetics of thermal decomposition of copper acetate in the oxidative environment by the STA method and established that the intensive weight loss of this substance occurred in the temperature interval 170–309 °C. This process of decomposition of copper acetate was characterized by the presence of several reflexes on the DTG profile (Zhang et al. 2005), which is in good agreement with data of Fig. 4.

The combustion dynamic analysis results also support abovementioned conclusions. The variation in activation energy values with particle size is insignificant. It indicates, that the nature of occurring chemical reactions is practically same, regardless particle size. Generally, the activation energy of initial sample was varied in range of 142–158 kJ/mol, for sample modified by mechanical method (100–124 kJ/mol), for sample modified by wet impregnation (5464 kJ/mol). Similar results were observed for both temperatures of onset and end of combustion, indicating the significant contribution of reaction rate in combustion enhancement.

According to the MS analysis, decomposition of copper acetate was accompanied by CO_2 emissions ($m/z = 44$). This can be clearly observed for the mechanically modified samples, which exhibit an additional peak in the temperature range of 210–320 °C. This effect is most likely associated with a lower dispersion and non-uniform distribution of the additive in the sample composition (Fig. 3). Thus, the formation of additional exothermic reflections in the low-temperature part of the oxidation process for the samples modified with copper acetate is associated with the staged decomposition of the additive, both on the surface of anthracite particles and in their bulk. As the size of anthracite particles increases, the intensity of copper acetate thermolysis grows, which is evidenced by the increased maximum oxidation rate.

It should be noted that the effect of copper acetate on oxidation is also expressed in the decreased T_{max}, when the oxidation reaction rate attains its maximum. The most significant changes in T_{max} are found for the anthracite samples modified by incipient wetness impregnation (Table 3). It is also worth noting that a decrease in the maximum reaction rate w_{max} was observed. It differs from the case

of metal oxides, which usage causes an increase in the w_{max} values. It was previously demonstrated by Gong et al. (2010a; 2010b) and Zhang et al. (2020).

3.3 Ignition and combustion

Figure 6 shows a histogram that illustrates the dependence of the ignition delay time on the size of anthracite particles and modification method.

As can be seen in Fig. 6, an increase in the size of anthracite particles (from 0.1 to 2.0 mm) of the samples leads to a linear increase in the ignition delay time (τ_i). An increase in the ignition delay time with a size of fuel particles was also observed by other authors (Adeosun et al. 2018). On the one hand, this is due to the decreased specific surface area of the particles and increased interparticle space (Fig. 1). On the other hand, an increase in the size of fuel pellets leads to degradation of the process kinetics that is associated with an increase in the energy needed for initiation of the volatile matter release. Given the previously mentioned similarity of chemical oxidation reactions, the observed differences in the τ_i values are most likely associated with the transition of the process from a kinetic mode (as in thermal analysis) to a diffusion one at temperature increased up to 800 °C. The use of additive $Cu(CH_3COO)_2 \cdot H_2O$, regardless of the method of its introduction and fractional composition,

Fig. 6 Ignition delay time for the initial and modified anthracite samples of different fractions. ref refers to reference sample, mech refers to sample modified by mechanical activation method, impreg refers to sample modified by incipient wetness impregnation method. The data are retrieved by high-speed video recording. The heating medium temperature $T_g = 800$ °C, the sample weight is approx. 0.1 g. The labeling (***) means statistically significant difference for each fraction ($p < 0.001$)

reduces the ignition delay time τ_i on average by 38%. Activation of the ignition induced by copper acetate is associated with its thermal decomposition, accompanied by formation of acetone vapors, acetaldehyde and acetic acid (Arii and Masuda 1999). Thus, oxidation of gas-phase decomposition products of copper acetate is exothermic (Arii and Masuda 1999; Richardson 2000) and proceeds with additional heat generation.

Anthracite ignition activated by copper acetate can also be due to a change in the oxidative properties of the fuel and its composition, which is expressed in increased O/C and H/C values (Table 2).

The strongest effect of the additive characterized by maximum reduction in τ_i (approx. 2.4 fold) is achieved by using the smallest fraction of anthracite (with particle size $d < 0.1$ mm), provided that it is modified by incipient wetness impregnation. For the latter, an increased catalytic effect can be observed due to a higher dispersion of the additive, as well as its more uniform distribution in the fuel (Fig. 3). This may also be associated with a deeper penetration of the additive into the volume of the porous structure of anthracite particles during impregnation. This leads to formation of an additional amount of gas-phase products during thermal decomposition of copper acetate, which contributes to expansion of internal pores and channels followed by intensification of the volatile matter release.

The obtained results illustrating the ignition activation were compared for different anthracite fractions. It should be noted that the reduced effect of the additive with larger particles may be associated with a changed porosity of the fuel layer (Table 1). The free space expansion (porosity increase) between anthracite particles (Fig. 1) decreases the impact of the gas-phase fuel ignition reactions during the copper acetate thermolysis. This is due to the lack of interparticle space that prevents an increase in the local concentration of combustible gases in the bulk of the fuel layer. The dependence of the τ_i change (Fig. 6) on the particle size generally correlates with T_i (Table 3, Fig. 5) calculated using the thermal analysis data (Fig. 4).

Analysis of the mean-square deviation of the resulting τ_i values (Fig. 6) shows that the widest scatter in values is typical of the anthracite samples modified by mechanical mixing. This is due to a wide range of copper acetate particle sizes and heterogeneity of their distribution in the fuel (Fig. 3).

Figures 7 and 8 show typical high-speed video images that illustrate ignition. The data are presented for fractions $d < 0.1$ mm and $d = 1.0–2.0$ mm.

The ignition mechanism of the initial samples includes a set of the following sequential and parallel stages: heating, autogenous combustion, thermal destruction with the volatile matter release, mixing of flammable gases with an oxidizing medium and gas-phase ignition. In this case, the
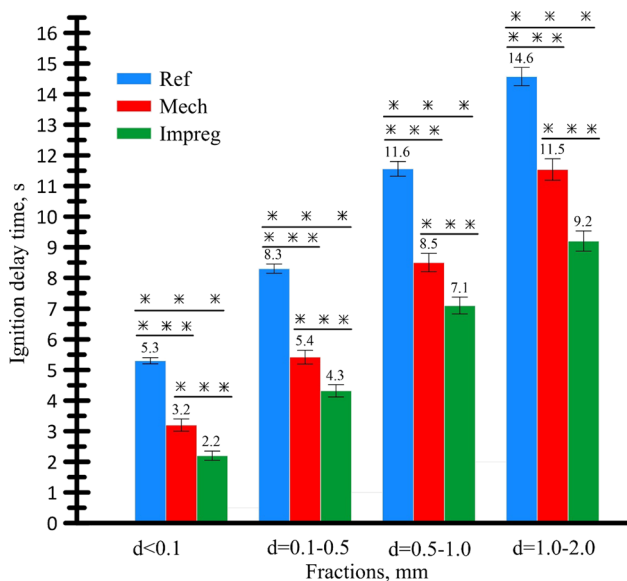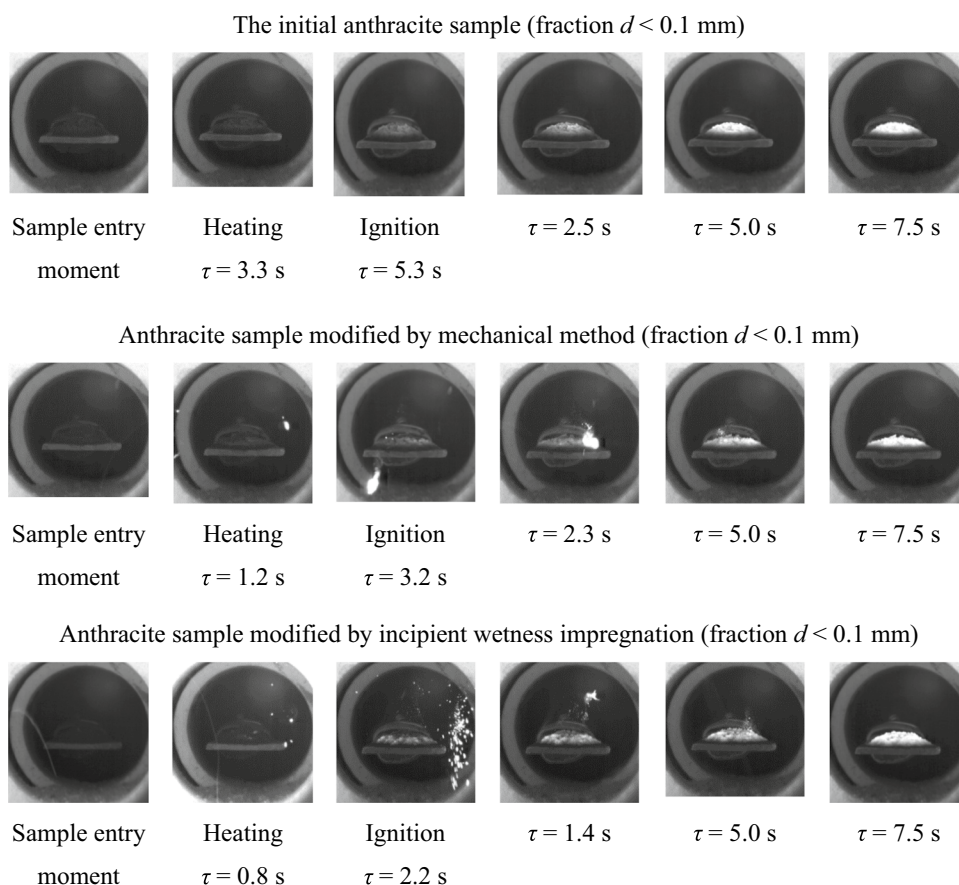
The initial anthracite sample (fraction $d < 0.1$ mm)

| Sample entry | Heating | Ignition | $\tau = 2.5$ s | $\tau = 5.0$ s | $\tau = 7.5$ s |
| moment | $\tau = 3.3$ s | $\tau = 5.3$ s | | | |

Anthracite sample modified by mechanical method (fraction $d < 0.1$ mm)

| Sample entry | Heating | Ignition | $\tau = 2.3$ s | $\tau = 5.0$ s | $\tau = 7.5$ s |
| moment | $\tau = 1.2$ s | $\tau = 3.2$ s | | | |

Anthracite sample modified by incipient wetness impregnation (fraction $d < 0.1$ mm)

| Sample entry | Heating | Ignition | $\tau = 1.4$ s | $\tau = 5.0$ s | $\tau = 7.5$ s |
| moment | $\tau = 0.8$ s | $\tau = 2.2$ s | | | |

ignition of the initial samples occurs without a visible flame similarly to that in (Wang et al. 2020), since the content of the volatile matter anthracite is low (Table 1), and the threshold concentrations required for ignition in the generated mixture of combustible gases (CO, CH$_4$, H$_2$, H$_2$S) near the sample are not reached. In turn, the ignition of the modified samples is accompanied by an additional stage of copper acetate decomposition.

The ignition of the initial samples occurs on the surface of the layer without a distinct local zone. Over time (after the sample ignition), the luminosity intensity increases due to an increase in the combustion temperature, which was demonstrated by Pinchuk et al. (2019).

Modified samples, together with the early ignition (Fig. 6) and decreased minimum temperature (Fig. 5), show an intensive propagation of the combustion front. A significant difference in the ignition and subsequent combustion of the modified samples of various fractions can be clearly seen in the time intervals of micro-explosions caused by decomposition of copper acetate and emission of combustible gas-phase products. For samples with a larger fraction (Fig. 8), micro-explosions predominantly precede the ignition of the fuel sample that is consistent with the thermal analysis data (Fig. 4). For samples with

a fraction $d < 0.1$ mm, micro-explosions are observed during combustion (Fig. 7). This can be due to the higher dispersion of particles (Fig. 1), which need a lower amount of energy for ignition and, as a consequence, a lower concentration of CO formed during decomposition of $Cu(CH_3COO)_2$. For samples with fine fractions ($d < 0.1$ mm), an intense emission of gas-phase decomposition products of copper acetate brings dispersed particles into a suspended state. Interaction between the oxidizing medium and the combustible decomposition products of copper acetate promotes the ignition of particles near the fuel sample (Fig. 7). The release of additional heat promotes the ignition reactions followed by the combustion of larger particles. In turn, for samples with a fraction $d = 1.0$–2.0 mm, micro-explosions change the shape of the fuel sample (Fig. 8), thereby intensifying the oxidation process. Bai et al. (Bai et al. 2017) reported that not only size, but also shape and roughness of particle make a significant contribution to its burning. Another important aspect affecting the action of activating additives is the type of used coals, which can vary in the content of carbon and volatile compounds (Larionov et al. 2021b, 2021a).

Comparison of the high-speed video recording images of ignition and combustion of the anthracite samples modified

Fig. 8 High-speed video images of the anthracite sample (fraction d = 1.0–2.0 mm) ignition. The heating medium temperature T_g = 800 °C, the sample weight is approx. 0.1 g

The initial anthracite sample (fraction d = 1.0–2.0mm)

Sample entry moment | τ = 2.5 s | τ = 5.4 s | τ = 7.5 s | T = 10.0 s | Ignition τ = 14.6 s

Anthracite sample modified by mechanical method (fraction d = 1.0–2.0 mm)

Sample entry moment | τ = 2.5 s | τ = 5.4 s | T = 8.3 s | τ = 10.0 s | Ignition τ = 11.5 s

Anthracite sample modified by incipient wetness impregnation (fraction d = 1.0–2.0 mm)

Sample entry moment | τ = 2.5 s | τ = 5.4 s | τ = 7.9 s | Ignition τ = 9.2 s | τ = 10.3 s
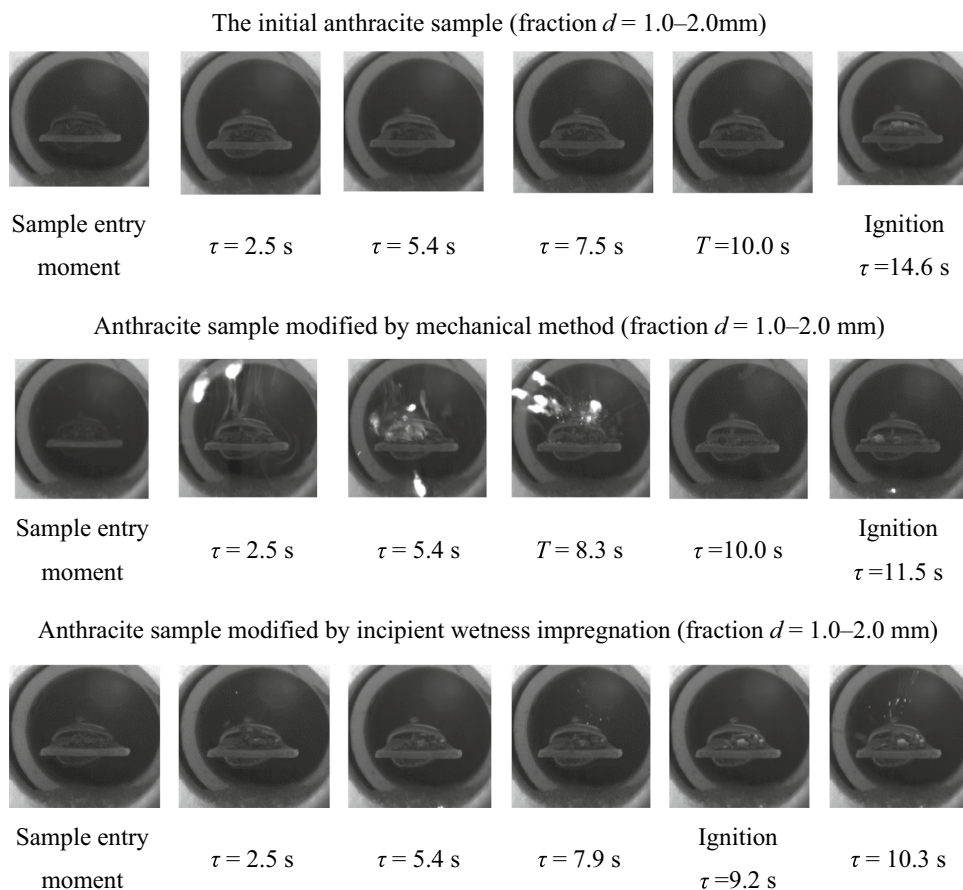
by different methods revealed longer time intervals of the periodic formation of micro-explosions with a stronger detonation effect in mechanical mixing. This is due to the different dispersion of copper acetate (Fig. 3).

These differences can be observed on micro photos (Fig. 9) illustrating partially oxidized anthracite particles in the samples with a fraction d = 0.5–1.0 mm in the combustion chamber (Fig. 2) at T_g = 800 °C. The samples exposure period from the moment of the sample entry was 15 s.

The mass change in the samples after their partial oxidation varied from 9.4 wt% to 19.2 wt% (Fig. 9), which is consistent with the thermal analysis data (Fig. 4). An activating

additive significantly changes the particle surface relief, where open channels and deep cavities are formed due to copper acetate decomposition and intensification of the volatile matter release.

As can be seen, the particle roughness depends on additive introduction method. Mechanical mixing leads to the formation of large-size channels and cavities (Fig. 9b). Incipient wetness impregnation leads to the formation of a loose surface with a large number of small cavities (Fig. 9c). The observed differences are apparently associated with a higher dispersion of the additive and its more uniform distribution in the sample composition (Fig. 3).
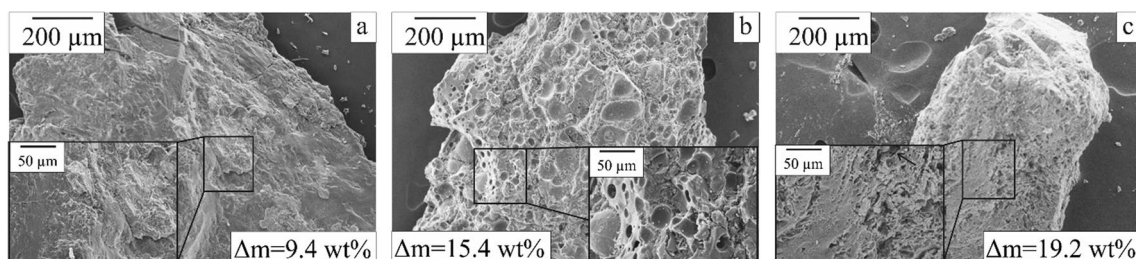
200 µm | 50 µm | a | Δm=9.4 wt% 200 µm | 50 µm | b | Δm=15.4 wt% 200 µm | 50 µm | c | Δm=19.2 wt%

Fig. 9 Micro photos of anthracite particles in the composition of partially oxidized samples (fraction d = 0.5–1.0 mm). **a** Reference sample **b** Mechanical mixing **c** Incipient wetness impregnation

As demonstrated in (Zhang et al. 2020), the intensification of coal oxidation with metal oxides also contributes to a significant development of pores and cracks formation. It is reflected in a more complete burnout of the carbon residue.

3.4 Fuel underburning

Figure 10 shows the data of the thermal and mass spectrometric analysis of the ash residue formed after the sample combustion performed using the experimental stand (Fig. 2).

According to the TG data, the mass loss of the samples was observed in the temperature range of 490–780 °C, which is associated with oxidation of the unburned carbon (fuel underburning) in the ash composition. This is evidenced by the formation of CO_2 revealed by the mass spectrometric analysis ($m/z = 44$). The profiles that characterize CO_2 emission exhibit a monomodal form and are found in the temperature range of 460–820 °C.

It should be noted that the increased particle size (of the sample) leads to an increase in fuel underburning on average by 2.8 wt%. Modified samples show decreased fuel underburning, which is accompanied by a lower intensity of CO_2 emission. This is associated with an active development of the particle surface (Fig. 9) and subsequent involvement of the resulting copper oxide in catalytic oxidation. For samples modified by incipient wetness impregnation, a smaller amount of carbon residue is found, which is due to a more efficient distribution of the activating additive in the anthracite structure (Fig. 3). According to Kapustyanskii (2014), fuel underburning is reduced as a result of catalytic coal combustion.

3.5 Composition of gas-phase products

Figures 11 and 12 show the concentration profiles characterizing the change in the concentration of different
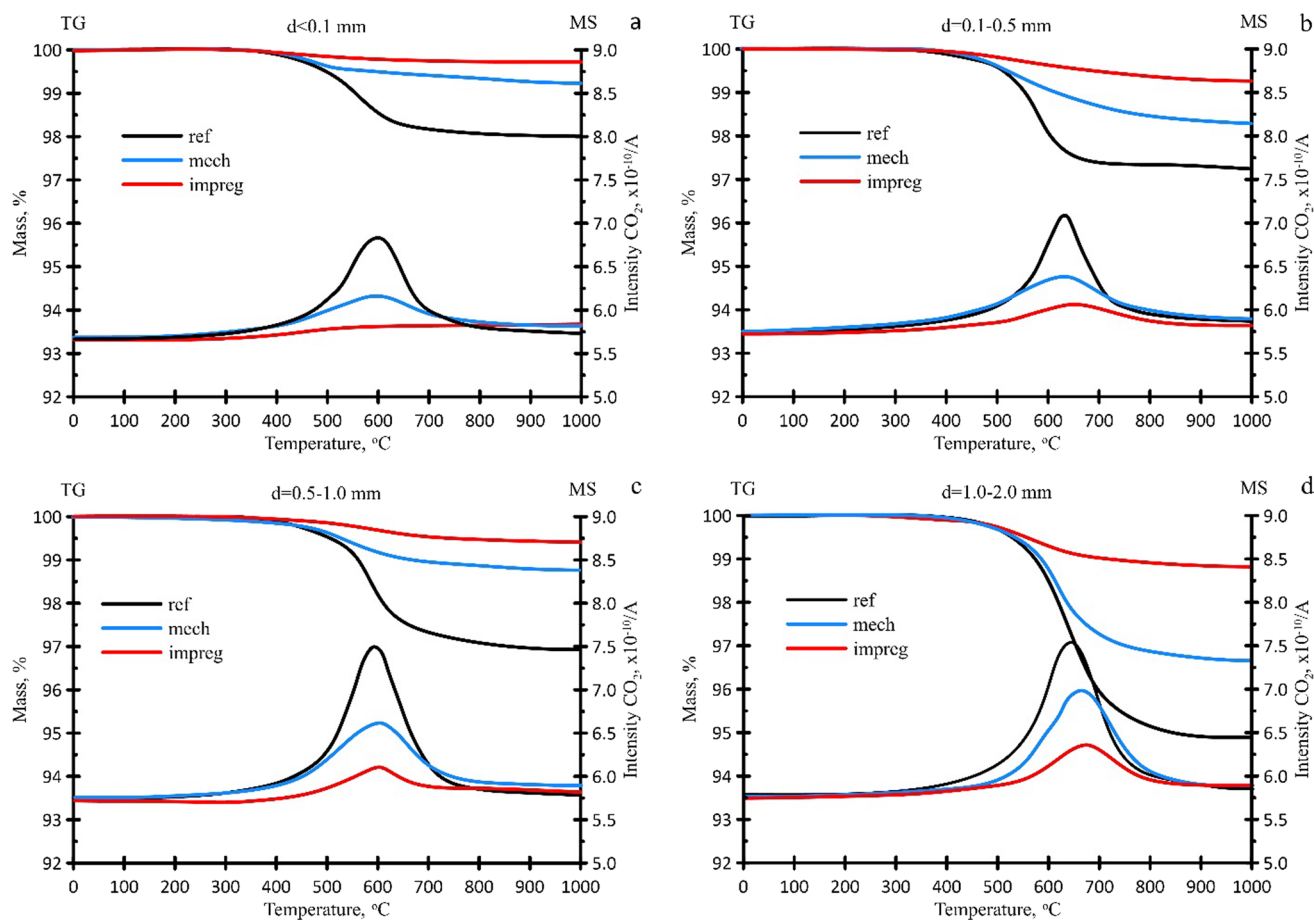
Fig. 10 TG and MS data for oxidation of the ash residue formed after combustion of different fractions of anthracite sample performed using the experimental stand. **a** $d < 0.1$ mm **b** $d = 0.1$–0.5 mm **c** $d = 0.5$–1.0 mm **d** $d = 1.0$–2.0 mm. ref means reference sample, mech means sample modified by mechanical activation method, impreg means sample modified by incipient wetness impregnation method. Heating gas (air) with a flow rate of 150 mL/min, heating rate is 10 °C/min
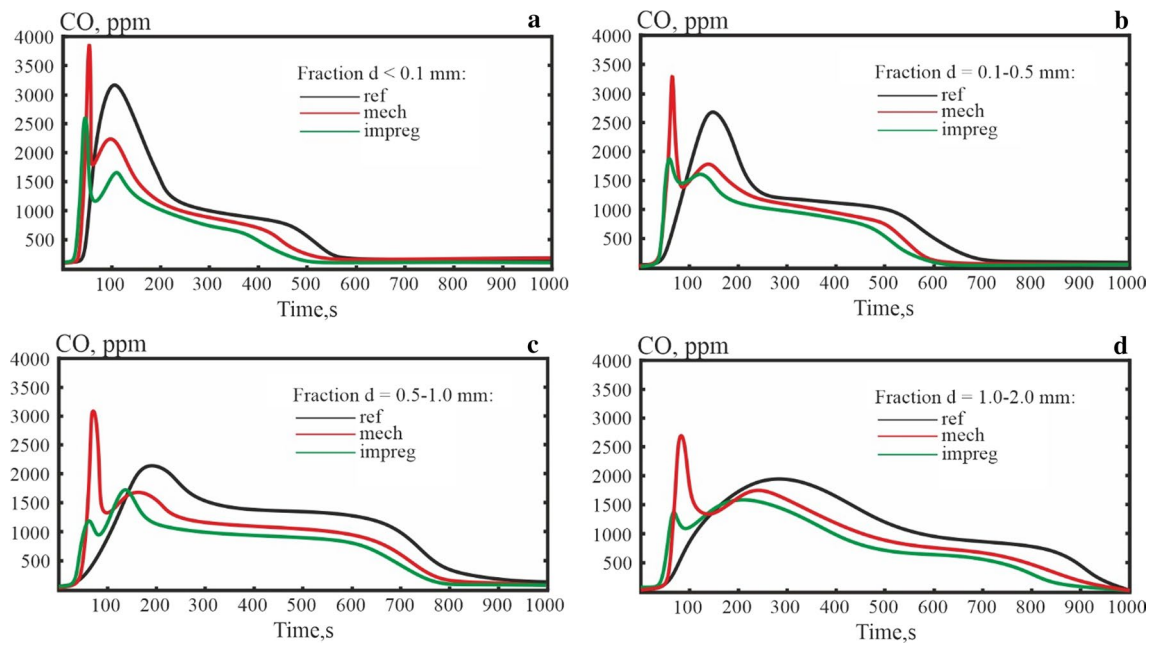
Fig. 11 Concentration profiles of CO emissions during combustion of anthracite samples of different fraction. **a** $d < 0.1$ mm **b** $d = 0.1$–0.5 mm **c** $d = 0.5$–1.0 mm **d** $d = 1.0$–2.0 mm. ref means reference sample, mech means sample modified by mechanical activation method, impreg means sample modified by incipient wetness impregnation method. The heating medium temperature $T_g = 800$ °C, the sample weight is approx. 0.1 g
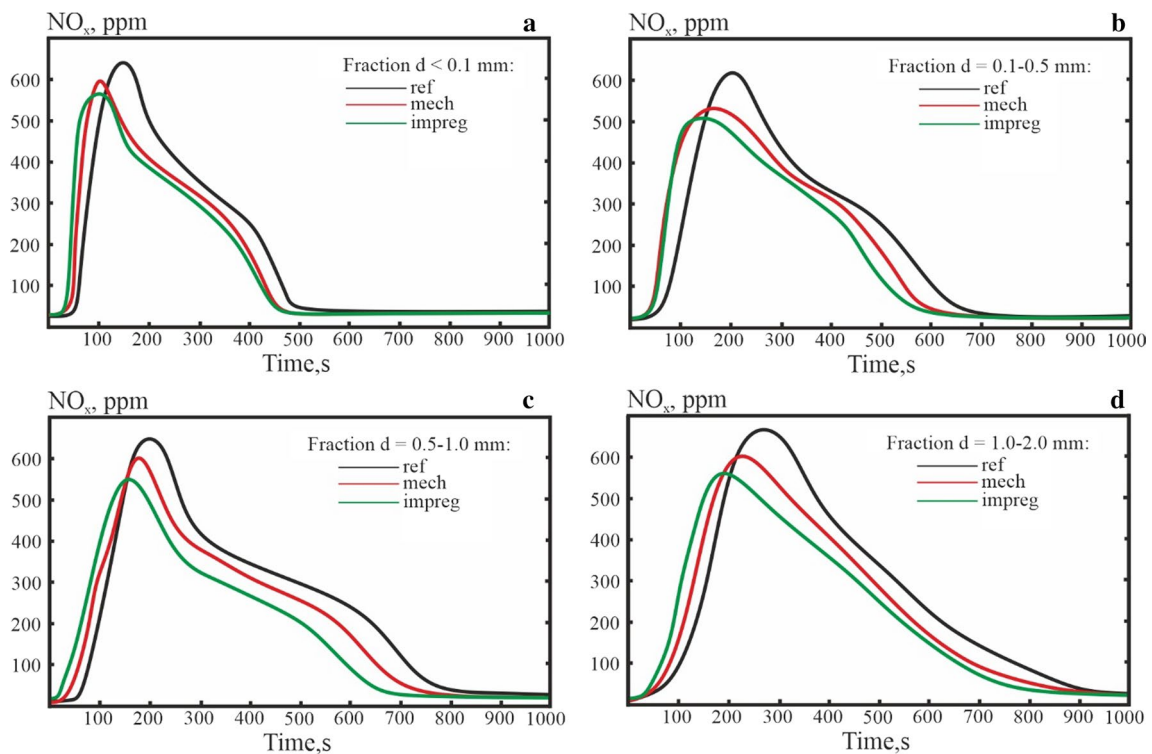

Fig. 12 Concentration profiles of NO_x emissions during combustion of anthracite samples of different fraction. **a** $d < 0.1$ mm **b** $d = 0.1$–0.5 mm **c** $d = 0.5$–1.0 mm **d** $d = 1.0$–2.0 mm. ref means reference sample, mech means sample modified by mechanical activation method, impreg means sample modified by incipient wetness impregnation method. The heating medium temperature $T_g = 800$ °C, the sample weight is approx. 0.1 g

components (CO and NO$_x$) in the formed gas-phase combustion products over time.

For all the samples studied, an increase in size of anthracite particles in the sample leads to an expansion of the time interval, during which CO and NO$_x$ are formed. For CO, a decrease in concentrated peaks can also be observed (Fig. 11) due to the change in the combustion kinetics.

In this case, the concentration profiles of the CO$_2$ emission – the main combustion product – were of a typical character. At the increased particle size, the pattern of the time interval change for the CO$_2$ profile was similar to the corresponding curves for CO and NO$_x$.

For all modified samples, the CO emission profile becomes bimodal. The first peak is associated with copper acetate decomposition. This is followed by the parallel stages of the volatile matter release and carbon residue oxidation, which is evidenced by the data presented in Figs. 4, 7 and 8. It should be noted that an increase in the particle size at the stage of copper acetate decomposition leads to a decrease in the intensity of CO evolution with a characteristic broadening of the peak, which may be due to the increased sample porosity and, as a consequence, to the changed conditions of the heat and mass transfer. For the samples modified with copper acetate by incipient wetness impregnation, lower concentrations of CO and NO$_x$ are observed in the composition of gas-phase products (Figs. 11 and 12, respectively). A decreased CO concentration is due to the combustion intensification that results in oxidation of CO to CO$_2$. A decreased NO$_x$ concentration is associated with a slight decrease in the nitrogen content in the fuel (Table 2) and weaker involvement of molecular nitrogen of air into anthracite combustion. As reported by Dorokhov et al. (2021), the combustion intensification is followed by a nonlinear decrease in the concentration of nitrogen oxide present within the gas-phase combustion products.

Table 4 presents the values of the relative integrand areas for the CO and NO$_x$ concentration curves in gas-phase combustion products.

As can be seen, an increase in the anthracite particle size increases the ratios S^{CO}_{MS}/S^{CO}_{ref} and $S^{NOx}_{MS}/S^{NOx}_{ref}$ caused by the changed sample porosity (Table 1) and combustion kinetics. In addition, incipient wetness impregnation results in the maximum decrease in the CO/NO$_x$

emission ratio (decreased $S^{CO}_{MS}/ S^{CO}_{ref}$ and $S^{NOx}_{MS}/S^{NOx}_{ref}$). This can be attributed to the increased activation capacity of the additive caused by its increased dispersion and more uniform distribution in the fuel composition (Fig. 3). A similar effect described in (Wu et al. 2021; Lei et al. 2021a) was assigned to the decreased release of nitrogen oxides associated with the activating additives used.

3.6 Activated combustion mechanism

Figure 13 presents a schematic overview of the probable mechanism of the activated ignition and combustion of anthracite promoted by the copper acetate.

The activation mechanism of ignition and subsequent combustion of anthracite impregnated with Cu(CH$_3$COO)$_2$ can be described by two stages. The first stage implies ignition that proceeds simultaneously with decomposition of the supported copper acetate. If larger particles are used, ignition follows the copper acetate decomposition (Fig. 7). During intensive formation of gas-phase decomposition products of copper acetate (acetone vapors, acetaldehyde, acetic acid and carbon monoxide), the pores and channels of the particles expand through the fuel sample layer, which intensifies the volatile matter release and development of the particle surface (Fig. 9). Thermolysis of Cu(CH$_3$COO)$_2$ is accompanied by the formation of copper oxide as the solid product. Upon reaching the threshold concentrations in combustible gas-phase products, the gas-phase ignition of the anthracite particles occurs, which is followed by propagation of the combustion reaction throughout the entire volume of the fuel sample.

The second stage refers mainly to the catalytic combustion of anthracite, which is promoted by the previously formed copper oxide. It is worth noting that the thermal degradation of copper acetate accomplishes with the formation of dispersed non-stoichiometric copper oxide Cu$_x$O, which may contain a set of different phases. Its further interaction with air leads to stabilization of the primary phase – CuO. The dispersed Cu$_x$O particles present both on the surface and in the bulk of the anthracite structure accelerate combustion, since copper oxide is a well-known to serve as an active catalyst for the complete oxidation of carbon (Liu et al. 2011). The oxygen species activated on the surface of copper oxide

Table 4 The relative value of the integrand areas of the peaks characterizing emission of CO and NO$_x$ for the initial (S^{CO}_{ref} and S^{NOx}_{ref}) and modified (S^{CO}_{MS} and S^{NOx}_{MS}) samples

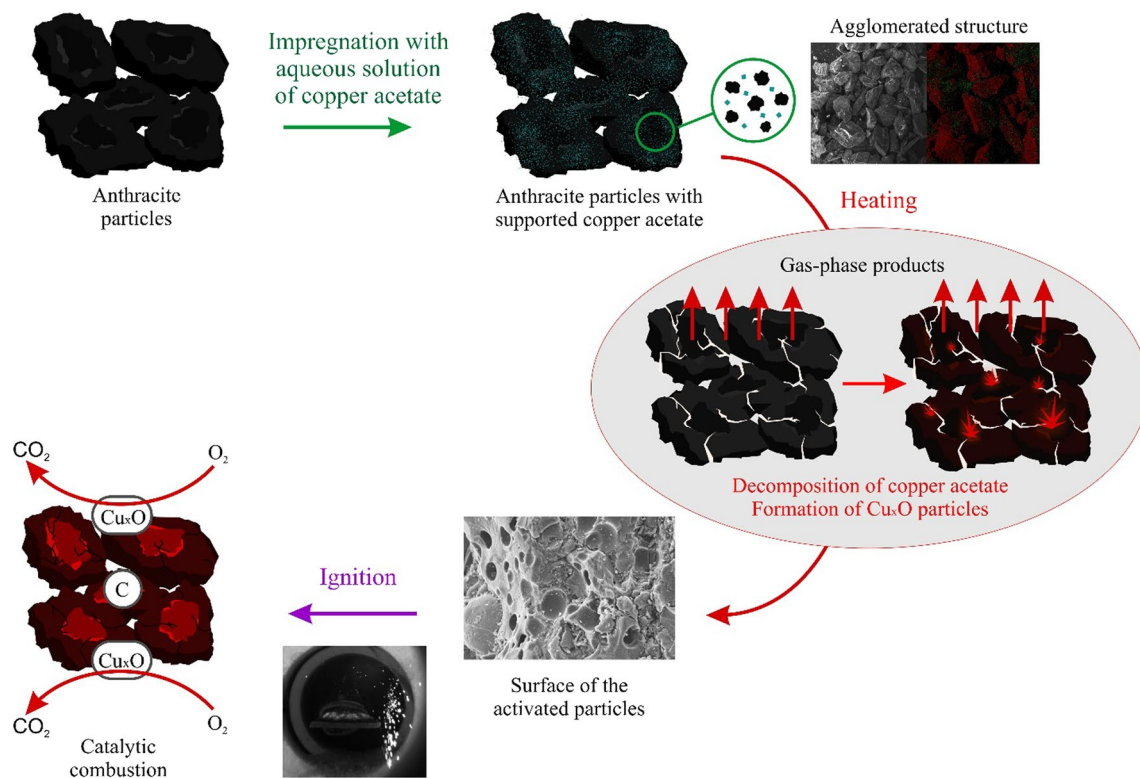| Sample preparation method	Particle size range (mm)							
	<0.1	0.1–0.5	0.5–1.0	1.0–2.0	<0.1	0.1–0.5	0.5–1.0	1.0–2.0
	S^{CO}_{MS}/S^{CO}_{ref}				$S^{NOx}_{MS}/S^{NOx}_{ref}$			
Mechanical treatment	0.79	0.82	0.89	0.93	0.73	0.79	0.90	0.87
Incipient wetness impregnation	0.70	0.68	0.84	0.87	0.71	0.74	0.77	0.83

Fig. 13 A schematic diagram of the possible mechanism for activating the ignition and combustion of anthracite by copper acetate

are characterized by a high mobility and an ability to oxidize the carbonaceous substrate. In turn, the interaction of copper oxide and carbon material is accompanied by electron density transfer, which contributes to additional activation of the oxidized substrate.

It is worth adding, that copper oxide exhibits a higher thermal conductivity (33–36 W/(m K)) (Zhang et al. 2005) relative to anthracite (0.134 W/(m K)) (Kuznetsov et al. 2022). Thus, the sample containing copper oxide shows faster heating of the fuel composition, which has a positive effect on the process kinetics.

In contrast to mechanical mixing, incipient wetness impregnation provides a higher dispersion of copper acetate and, therefore, a closer contact with the particle surface in the agglomerated structure (Fig. 3). For this modification, the formed combustible gas-phase products of thermal decomposition of $Cu(CH_3COO)_2$ pass through the entire volume of the fuel sample, thereby being involved in the gas-phase ignition of the anthracite particles.
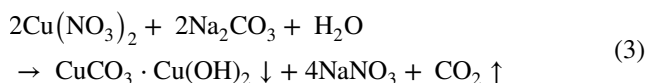
3.7 Copper recovery

The recovery of transitional metals from coal ash has become extremely relevant recently due to development of chemical looping combustion technologies and inevitable entrainment of the part of oxygen carrier material due to attrition (Staničić et al. 2021; Dai and Whitty 2022). The copper oxide is very promising substance as an oxygen carrier (Qasim et al. 2021), so several studies on its recovery from ash are presented in the literature. The most obvious solution is using different solvents for extraction (Karlfeldt Fedje et al. 2012; Lassesson et al. 2014), but there are also some alternative methods (Yoshino et al. 2015). While majority of such studies devoted to copper extraction from municipal solid waste ash (Karlfeldt Fedje et al. 2012; Lassesson et al. 2014), some authors proposed applying similar methods to coal ash proving their feasibility (Tao et al. 2014; Bojinova and Teodosieva 2016). The brief economic evaluation of using aluminum as an additive for promoting combustion of coal-water fuel presented by Valiullin et al. (2017) revealed efficiency of this approach.

As a result of the anthracite combustion with copper acetate additive, copper oxide is appeared within the ash residue composition. For the ash processing, the CuO can be extracted and used as an oxidation catalyst (Zhang et al. 2005). Additionally, some copper salts, such as nitrate (Eq. (2)), carbonate (Eqs. (3)–(4)) or copper sulfate (Eq. (5)), can be manufactured.

$$CuO + 2HNO_3 \rightarrow Cu(NO_3)_2 + H_2O \tag{2}$$

$$2Cu(NO_3)_2 + 2Na_2CO_3 + H_2O$$
$$\rightarrow CuCO_3 \cdot Cu(OH)_2 \downarrow + 4NaNO_3 + CO_2 \uparrow \qquad (3)$$

$$CuCO_3 \cdot Cu(OH)_2 + CO_2 \rightarrow 2CuCO_3 + H_2O \qquad (4)$$

$$CuO + H_2SO_4 \rightarrow CuSO_4 + H_2O \qquad (5)$$
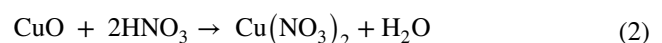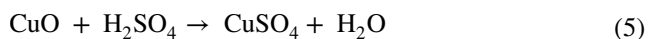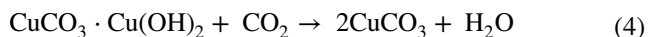
Both copper nitrate and sulfate are applicable for the coal combustion activations, as was demonstrated in our previous studies (Larionov et al. 2021a, 2021b).

3.8 Possible directions of potential application

According to an experimental research, copper acetate, as an activating additive, allows to increase the reactivity of solid fuel (Figs. 4–6). As a result, copper acetate can potentially be used as a launch activator of combustion, which will reduce the energy consumption for own needs during starting of the boiler units. Usually fuel oil or natural gas are used as launch fuels that require an additional number of technical solutions and auxiliary systems, as well as compulsory maintenance.

Due to reduced fuel under burning (Fig. 10) and a decreased concentration of the formed CO (Fig. 11), the application of copper acetate will also allow to obtain additional amount of heat during fuel burning. According to our estimates, the amount of useful heat released can be increased by 7%–10% depending on the fractional composition of the fuel and the method of applying the additive. For the latter, the most effective way is the impregnation method with preliminary dissolution of the additive in water and its application to fuel using irrigation systems. The application of this method will also ensure the explosion-proof operation of the fuel supply system by preventing dust formation during operation of coal feeders.

Thus, copper acetate in the form of an activating additive can potentially be used at coal energy facilities: heating boiler houses, condensation and cogeneration power plants. The most promising are objects on which coals with a high carbon content (including anthracite) are used via with moving bed-type boilers.

4 Conclusions

The aim of the present study was to explore the effect of the deposition method and the fuel particle size on the ignition and combustion properties of low reactivity anthracite with copper acetate as promoting additive. EDX mapping revealed that the incipient wetness impregnation method provides a higher dispersion and more uniform distribution of the activating agent in the sample than the mechanical mixing. Regardless to the introduction method and the particle size, the addition of copper acetate increases the reactivity of anthracite, which is expressed by the lower initial temperature of intensive oxidation ($\Delta T_i = 35$–190 °C) and the shorter ignition delay time ($\Delta \tau_i = 2.1$–5.4 s). The activation energy values were also decreased from -150 kJ/mol to -110 kJ/mol for mechanically introduced additive and to -60 kJ/mol for additive introduced by wet impregnation. It was associated with the copper acetate thermolysis and the emission of an additional amount of combustible gas-phase products. It was also observed that an early stage of the anthracite combustion is accompanied by periodic micro-explosions caused by the additive decomposition. The morphology of the particles was also changed. They become loosened, and the roughness of the particle surface is increased. The content of the unreacted carbon within the ash residue is decreased (by 77.3% in average), as well as emissions of CO and NO$_x$ are diminished in average by 18.5% and 20.8%, respectively. For the anthracite particles of a larger size, the promoting effect is weaker than for the smaller ones. These effects are observed in terms of both oxidation and combustion characteristics. For all the studied samples, regardless to the particle size, the effect of the additive introduced by an incipient wetness method is stronger than for the additive introduced by a mechanical mixing. A decrease in the characteristic oxidation temperatures for the impregnated samples is higher by 50–110 °C if compared with the ones prepared by the mechanical mixing. A decrease in the ignition delay time is also higher (by 30%–50%). Similar dependences are observed for emissions of the gas-phase combustion products. The lower particle size and the use of an incipient wetness impregnation method result in lowering the emissions. A two-stage mechanism for activating the ignition and subsequent combustion of anthracite has been proposed. The first stage implies copper acetate thermolysis, the emission of combustible gas-phase products and the subsequent intensification of the anthracite ignition with simultaneous development of the particle surface. The second stage includes the formation of the dispersed non-stoichiometric copper oxide species with higher thermal conductivity if compared with anthracite, which catalyze the oxidation of the solid fuel residue and increase the depth of the combustion process. The approaches for the copper recovery from the ash are proposed as well.

Author contributions L K.B.: Conceptualization, Methodology, Resources, Writing—Original Draft, Writing—Review & Editing, Funding acquisition, Project administration; M I.V.: Conceptualization, Validation, Writing—Original Draft, Writing—Review & Editing; B N.I.: Investigation, Data Curation; G A.S.: Investigation, Data Curation; K A.Zh.: Investigation, Data Curation; S K.V.: Methodology, Writing—Original Draft, Writing—Review & Editing; R A.S.:

Declarations

References

Abbasi-Atibeh E, Yozgatligil A (2014) A study on the effects of catalysts on pyrolysis and combustion characteristics of Turkish lignite in oxy-fuel conditions. Fuel 115:841–849. https://doi.org/10.1016/j.fuel.2013.01.073

Adeosun A, Xiao Z, Yang Z, Yao Q, Axelbaum RL (2018) The effects of particle size and reducing-to-oxidizing environment on coal stream ignition. Combust Flame 195:282–291. https://doi.org/10.1016/j.combustflame.2018.05.003

AlKetbi M, Polychronopoulou K, Abi Jaoude M, Vasiliades MA, Sebastian V, Hinder SJ, Baker MA, Zedan AF, Efstathiou AM (2020) Cu-Ce-La-Ox as efficient CO oxidation catalysts: effect of Cu content. Appl Surf Sci 505:144474. https://doi.org/10.1016/j.apsusc.2019.144474

Arii T, Masuda Y (1999) Thermal decomposition of calcium copper acetate hexahydrate by simultaneous measurement of controlled-rate thermogravimetry and mass spectrometry (CRTG–MS). Thermochim Acta 342:139–146. https://doi.org/10.1016/S0040-6031(99)00294-4

Bai X, Lu G, Bennet T, Sarroza A, Eastwick C, Liu H, Yan Y (2017) Combustion behavior profiling of single pulverized coal particles in a drop tube furnace through high-speed imaging and image analysis. Exp Therm Fluid Sci 85:322–330. https://doi.org/10.1016/j.expthermflusci.2017.03.018

Bojinova D, Teodosieva R (2016) Leaching of valuable elements from thermal power plant bottom ash using a thermo–hydrometallurgical process. Waste Manag Res J a Sustain Circ Econ 34:511–517. https://doi.org/10.1177/0734242X16633775

Dai J, Whitty KJ (2022) Evaluation of the energy balance of chemical looping combustion of solid fuels using CuO-based oxygen carriers. Fuel Process Technol 233:107285. https://doi.org/10.1016/j.fuproc.2022.107285

de las Obras-Loscertales M, Rufas A, de Diego LF, García-Labiano F, Gayán P, Abad A, Adánez J, (2013) Effects of temperature and flue gas recycle on the SO_2 and NO_x emissions in an Oxy-fuel fluidized bed combustor. Energy Procedia 37:1275–1282. https://doi.org/10.1016/j.egypro.2013.06.002

Dorokhov VV, Kuznetsov GV, Nyashina GS, Strizhak PA (2021) Composition of a gas and ash mixture formed during the pyrolysis and combustion of coal-water slurries containing petrochemicals. Environ Pollut 285:117390. https://doi.org/10.1016/j.envpol.2021.117390

Fedorov AV, Dubinin YV, Yeletsky PM, Fedorov IA, Shelest SN, Yakovlev VA (2021) Combustion of sewage sludge in a fluidized bed of catalyst: ASPEN PLUS model. J Hazard Mater 405:124196. https://doi.org/10.1016/j.jhazmat.2020.124196

Gong X, Zhang S (2017) Catalytic effects of CeO_2/Fe_2O_3 and inherent mineral matter on anthracite combustion reactions and its kinetic analysis. Energy Fuels 31:12867–12874. https://doi.org/10.1021/acs.energyfuels.7b02568

Gong X, Guo Z, Wang Z (2010a) Reactivity of pulverized coals during combustion catalyzed by CeO_2 and Fe_2O_3. Combust Flame 157:351–356. https://doi.org/10.1016/j.combustflame.2009.06.025

Gong X, Guo Z, Wang Z (2010b) Variation on anthracite combustion efficiency with CeO_2 and Fe_2O_3 addition by differential thermal analysis (DTA). Energy 35:506–511. https://doi.org/10.1016/j.energy.2009.10.017

Guo Q, Liu Y, Jia W, Yang M, Hu X, Ryu H-J (2014) Performance of Ca-based oxygen carriers decorated by K_2CO_3 or Fe_2O_3 for coal chemical looping combustion. Energy Fuels 28:7053–7060. https://doi.org/10.1021/ef5013006

He X-M, Qin J, Liu R-Z, Hu Z-J, Wang J-G, Huang C-J, Li T-L, Wang S-J (2013) Catalytic combustion of inferior coal in the cement industry by thermogravimetric analysis. Energy Sour, Part A Rec Util Environ Eff 35:1233–1240. https://doi.org/10.1080/15567036.2010.516324

Hu F, Li P, Zhang T, Li W, Wang K, Guo J, Mi J, Liu Z (2019) Reaction characteristics and MILD combustion of residual char in a pilot-scale furnace. Energy Fuels 33:12791–12800. https://doi.org/10.1021/acs.energyfuels.9b02962

Ismagilov ZR, Kerzhentsev MA (1999) Fluidized bed catalytic combustion. Catal Today 47:339–346. https://doi.org/10.1016/S0920-5861(98)00315-0

Kapustyanskii AA (2014) Effect of combustion catalyst on the operation efficiency of steam boilers. Therm Eng 61:666–670. https://doi.org/10.1134/S0040601514070040

Karlfeldt Fedje K, Ekberg C, Skarnemark G, Pires E, Steenari B-M (2012) Initial studies of the recovery of Cu from MSWI fly ash leachates using solvent extraction. Waste Manag Res J a Sustain Circ Econ 30:1072–1080. https://doi.org/10.1177/0734242X12441385

Köpsel RFW, Halang S (1997) Catalytic influence of ash elements on NOx formation in char combustion under fluidized bed conditions. Fuel 76:345–351. https://doi.org/10.1016/S0016-2361(96)00231-1

Kuznetsov GV, Malyshev DY, Syrodoy SV, Gutareva NY, Purin MV, Kostoreva ZA (2022) Ignition of bio-water-coal fuels based on coal and charcoal. Combust Sci Technol 194:1003–1026. https://doi.org/10.1080/00102202.2020.1799203

Larionov K, Slyusarskiy K, Tsibulskiy S, Tolokolnikov A, Mishakov I, Bauman Y, Vedyagin A, Gromov A (2020) Effect of $Cu(NO_3)_2$ and $Cu(CH_3COO)_2$ activating additives on combustion characteristics of anthracite and its semi-coke. Energies 13:5926. https://doi.org/10.3390/en13225926

Larionov KB, Mishakov IV, Slyusarskiy KV, Tsibulskiy SA, Tabakaev RB, Bauman YI, Vedyagin AA, Nalivaiko AY, Gromov

AA (2021a) Combustion of bituminous coal and semicoke with copper salts. Fuel Process Technol 213:106706

Larionov KB, Mishakov IV, Slyusarskiy KV, Vedyagin AA (2021b) Intensification of bituminous coal and lignite oxidation by copper-based activating additives. Int J Coal Sci Technol 8:141–153. https://doi.org/10.1007/s40789-020-00350-z

Lassesson H, Fedje KK, Steenari B-M (2014) Leaching for recovery of copper from municipal solid waste incineration fly ash: Influence of ash properties and metal speciation. Waste Manag Res J a Sustain Circ Econ 32:755–762. https://doi.org/10.1177/0734242X14542147

Lei Z, Liu M, Yan J, Chun T, Fang J, Li Z, Shui H, Ren S, Wang Z, Cao X, Kong Y, Kang S (2021a) Catalytic combustion of coke nuts and in-situ NO reduction under the action of steel scale. Fuel 289:119779. https://doi.org/10.1016/j.fuel.2020.119779

Lei Z, Yan J, Fang J, Shui H, Ren S, Wang Z, Li Z, Kong Y, Kang S (2021b) Catalytic combustion of coke and NO reduction in-situ under the action of Fe, Fe–CaO and Fe–CeO2. Energy 216:119246. https://doi.org/10.1016/j.energy.2020.119246

Li WB, Wang JX, Gong H (2009) Catalytic combustion of VOCs on non-noble metal catalysts. Catal Today 148:81–87. https://doi.org/10.1016/j.cattod.2009.03.007

Liu M, Lin MC, Wang C (2011) Enhancements of thermal conductivities with Cu, CuO, and carbon nanotube nanofluids and application of MWNT/water nanofluid on a water chiller system. Nanoscale Res Lett 6:297. https://doi.org/10.1186/1556-276X-6-297

Parmon VN, Simonov AD, Sadykov VA, Tikhov SF (2015) Catalytic combustion: achievements and problems. Combust Explos Shock Waves 51:143–150. https://doi.org/10.1134/S001050821502001X

Pinchuk VA, Kuzmin AV (2020) The effect of the addition of TiO_2 nanoparticles to coal-water fuel on its thermophysical properties and combustion parameters. Fuel 267:117220. https://doi.org/10.1016/j.fuel.2020.117220

Pinchuk V, Sharabura TA, Moumane M, Kuzmin A (2019) Experimental investigation of the influence of temperature, coal metamorphic stage, and of the size of coal–water fuel drop on the fuel drop combustion process. Int J Energy a Clean Environ 20:43–62. https://doi.org/10.1615/InterJEnerCleanEnv.2019030065

Qasim M, Ayoub M, Ghazali NA, Aqsha A, Ameen M (2021) Recent advances and development of various oxygen carriers for the chemical looping combustion process: a review. Ind Eng Chem Res 60:8621–8641. https://doi.org/10.1021/acs.iecr.1c01111

Riley C, Canning G, De La Riva A, Zhou S, Peterson E, Boubnov A, Hoffman A, Tran M, Bare SR, Lin S, Guo H, Datye A (2020) Environmentally benign synthesis of a PGM-free catalyst for low temperature CO oxidation. Appl Catal B Environ 264:118547. https://doi.org/10.1016/j.apcatb.2019.118547

Ryabov GA (2022) Chemical looping combustion and gasification of fuels. a review of studies and new process solutions. Therm Eng 69:26–41. https://doi.org/10.1134/S0040601521100062

Simonov AD, Fedorov NA, Dubinin YV, Yazykov NA, Yakovlev VA, Parmon VN (2013) Catalytic heat-generating units for industrial heating. Catal Ind 5:42–49. https://doi.org/10.1134/S2070050413010087

Staničić I, Cañete Vela I, Backman R, Maric J, Cao Y, Mattisson T (2021) Fate of lead, copper, zinc and antimony during chemical looping gasification of automotive shredder residue. Fuel 302:121147. https://doi.org/10.1016/j.fuel.2021.121147

Tao H-C, Lei T, Shi G, Sun X-N, Wei X-Y, Zhang L-J, Wu W-M (2014) Removal of heavy metals from fly ash leachate using combined bioelectrochemical systems and electrolysis. J Hazard Mater 264:1–7. https://doi.org/10.1016/j.jhazmat.2013.10.057

Tokareva IV, Mishakov IV, Vedyagin AA, Korneev DV, Petuhkova ES, Savvinova ME (2014) Modification of carbon fibers for reinforcing pipe polyethylene. Compos Nanostruct 6:158–167

Valiullin TR, Egorov RI, Strizhak PA (2017) Combustion of the waste-derived fuel compositions metallized by aluminium powder. Combust Flame 182:14–19. https://doi.org/10.1016/j.combustflame.2017.04.009

Wang C, Lei M, Yan W, Wang S, Jia L (2011) Combustion characteristics and Ash formation of pulverized coal under pressurized oxy-fuel conditions. Energy Fuels 25:4333–4344. https://doi.org/10.1021/ef200956q

Wang C, Bi H, Jiang X, Jiang C, Lin Q (2020) Experimental study on ignition and combustion of coal-rice husk blends pellets in air and oxy-fuel conditions. J Energy Inst 93:1544–1558. https://doi.org/10.1016/j.joei.2020.01.017

Wu Y, Pang Q, He Z, Song T, Zhan W, Zhang J (2019) Non-isothermal thermogravimetric investigation on mutual effect between bituminite and anthracite in blends for blast furnace injection. J Iron Steel Res Int 26:818–828. https://doi.org/10.1007/s42243-018-0198-9

Wu X, Liu Z, Fan W, Zhou C, Liu S, Chen J, Guo H (2021) Effect of metal elements in coal ash on NO release characteristics during oxy-fuel combustion at high temperature. J Energy Inst 94:107–119. https://doi.org/10.1016/j.joei.2020.11.005

Yang L, Luo H, Zhang K, Gong Z, Wu W (2019) Effect of limonite additive on combustion and NOx emission characteristics of anthracite. Meitan Xuebao/j China Coal Soc 44:305–312. https://doi.org/10.13225/j.cnki.jccs.2018.1703

Yoshino A, Yamato R, Sato K, Takarada T (2015) Cu recovery from industrial wastewater using brown coal. Fuel Process Technol 136:64–67. https://doi.org/10.1016/j.fuproc.2014.09.029

Zhang K, Hong J, Cao G, Zhan D, Tao Y, Cong C (2005) The kinetics of thermal dehydration of Copper (II) acetate monohydrate in air. Thermochim Acta 437:145–149. https://doi.org/10.1016/j.tca.2005.06.038

Zhang S, Chen Z, Chen X, Gong X (2014) Effects of ash/K_2CO_3/Fe_2O_3 on ignition temperature and combustion rate of demineralized anthracite. J Fuel Chem Technol 42:166–174. https://doi.org/10.1016/S1872-5813(14)60013-X

Zhang H, Dou B, Li J, Zhao L, Wu K (2020) Thermogravimetric kinetics on catalytic combustion of bituminous coal. J Energy Inst 93:2526–2535. https://doi.org/10.1016/j.joei.2020.08.012

Zhang X, Chen Z, Li L, Zeng L, Li Z (2022) Industrial-scale investigations on combustion characteristics and NO$_x$ emissions of a 300-MW e down-fired boiler: bituminous coal combustion and coal varieties comparison. Combust Sci Technol 194:3155–3174. https://doi.org/10.1080/00102202.2021.1912028

Zhao GW, Yu WQ, Xiao YH (2011) Study on brown coal pyrolysis and catalytic pyrolysis. Adv Mater Res 236–238:660–663. https://doi.org/10.4028/www.scientific.net/AMR.236-238.660

Zou C, Zhao J, Li X, Shi R (2016) Effects of catalysts on combustion reactivity of anthracite and coal char with low combustibility at low/high heating rate. J Therm Anal Calorim 126:1469–1480. https://doi.org/10.1007/s10973-016-5806-y

British petroleum (2020) Statistical review of world energy 2021. In: BP energy outlook 2020. https://www.bp.com/en/global/corporate/energy-economics/statistical-review-of-world-energy/electricity.html. Accessed 25 Nov 2020

IEA (2020) Electricity 2020. https://www.iea.org/fuels-and-technologies/electricity. Accessed 25 Nov 2020

IEA (2021) Net zero by 2050. OECD

Richardson HW (2000) Copper compounds. In: ullmann's encyclopedia of industrial chemistry. Wiley, Germany